Remote Sensing of Environment 113 (2009) 635–644

Contents lists available at ScienceDirect

Remote Sensing of Environment

journal homepage: www.elsevier.com/locate/rse

Evaluation of MODIS SWIR and NIR-SWIR atmospheric correction algorithms using SeaBASS data

Menghua Wang [a,*], SeungHyun Son [a,b], Wei Shi [a,c]

[a] NOAA National Environmental Satellite, Data, and Information Service, Center for Satellite Applications and Research, E/RA3, Room 102, 5200 Auth Road, Camp Springs, MD 20746, USA
[b] I.M. Systems Group, Rockville, MD, USA
[c] CIRA at Colorado State University, Fort Collins, CO, USA

ARTICLE INFO

Article history:
Received 2 June 2008
Received in revised form 18 August 2008
Accepted 8 November 2008

Keywords:
Ocean color remote sensing
Atmospheric correction for turbid waters
Algorithm validation

ABSTRACT

Using the NASA maintained ocean optical and biological *in situ* data that were collected during 2002–2005, we have evaluated the performance of atmospheric correction algorithms for the ocean color products from the Moderate Resolution Imaging Spectroradiometer (MODIS) on Aqua. Specifically, algorithms using the MODIS shortwave infrared (SWIR) bands and an approach using the near-infrared (NIR) and SWIR combined method are evaluated, compared to the match-up results from the NASA standard algorithm (using the NIR bands). The *in situ* data for the match-up analyses were collected mostly from non-turbid ocean waters. It is critical to assess and understand the algorithm performance for deriving MODIS ocean color products, providing science and user communities with the important data quality information. Results show that, although the SWIR method for data processing has generally reduced the bias errors, the noise errors are increased due mainly to significantly lower sensor signal-noise ratio (SNR) values for the MODIS SWIR bands, as well as the increased uncertainties using the SWIR method for the atmospheric correction. This has further demonstrated that future ocean color satellite sensors will require significantly improved sensor SNR performance for the SWIR bands. The NIR–SWIR combined method, for which the non-turbid and turbid ocean waters are processed using the NIR and SWIR method, respectively, has been shown to produce improved ocean color products.

Published by Elsevier Inc.

1. Introduction

In a recent development, an atmospheric correction algorithm using the shortwave infrared (SWIR) bands has been demonstrated to derive improved ocean color products in turbid coastal waters measured by the Moderate Resolution Imaging Spectroradiometer (MODIS) on Aqua (Franz et al., 2006; Wang, 2007; Wang and Shi, 2005; Wang et al., 2007). The NASA standard ocean color products have been routinely derived using the two MODIS near-infrared (NIR) bands (748 and 869 nm) for atmospheric correction (Gordon, 1997; Gordon and Wang, 1994), with assumption of a black ocean in the NIR for the open ocean and modifications to account for the NIR ocean contributions for productive (but not very turbid) near-shore or coastal waters (Stumpf et al., 2003). The same data processing procedure has also been used for deriving ocean color products from the Sea-viewing Wide Field-of-view Sensor (SeaWiFS) (Gordon and Wang, 1994; McClain et al., 2004; Wang et al., 2005). For turbid waters in coastal regions, however, the NIR black ocean assumption and modifications are often invalid (Lavender et al., 2005; Ruddick et al., 2000; Siegel et al., 2000; Stumpf et al., 2003; Wang and Shi, 2005), leading to large errors in the MODIS-derived ocean color products (Wang et al., 2007). With the *in situ* measurements from the China east coastal region, Wang et al. (2007) demonstrated that using the SWIR algorithm the MODIS ocean color products can be improved in the extremely turbid waters. However, there are some noise errors in the SWIR-derived data due mainly to the considerably lower sensor signal-noise ratio (SNR) values for the MODIS SWIR bands (Wang and Shi, 2007). Based on MODIS specifications (http://modis.gsfc.nasa.gov/), for a case of maritime aerosols with aerosol optical thickness of 0.1 at the NIR band, the MODIS SNR values for the two NIR ocean bands (1 km spatial resolution) 748 and 869 nm are 341 and 272, respectively, while the SNR values are 12, 12, and 11 for the three SWIR bands (0.5 km spatial resolution) at 1240, 1640, and 2130 nm, respectively (Wang, 2007). In fact, for accurate atmospheric correction for ocean color products, it requires an order of magnitude larger in the SNR values than those in the MODIS SWIR band specifications (Wang, 2007). With the spatial resolution of 1 km for the MODIS SWIR bands, the SWIR SNR values can be increased, but still not enough. Future satellite sensor, the Visible Infrared Imaging Radiometer Suite (VIIRS) on board of the National Polar-Orbiting Operational Environmental Satellite System (NPOESS), will also have similar three SWIR bands as MODIS. Unfortunately, the VIIRS SWIR bands were also designed for the land and atmosphere applications with low

* Corresponding author. Tel.: +1 301 763 8102; fax: +1 301 763 8572.
E-mail address: Menghua.Wang@noaa.gov (M. Wang).

0034-4257/$ – see front matter. Published by Elsevier Inc.
doi:10.1016/j.rse.2008.11.005

SNR characteristics. Recently, a NIR–SWIR combined method for the MODIS ocean color data processing has been proposed (Shi and Wang, 2007; Wang and Shi, 2007). For this approach, ocean color products are derived using the standard (NIR) algorithm in non-turbid oceans, whereas for turbid waters the products are obtained using the SWIR method. Therefore, it is useful to evaluate these two new approaches, i.e., the SWIR and NIR–SWIR combined methods, for deriving the ocean color products. Note that both SWIR and NIR–SWIR algorithms use the MODIS SWIR reflectance at the wavelength 1240 nm for the cloud masking (Wang and Shi, 2006), as well as the improved aerosol lookup tables that include the aerosol polarization effects (Wang, 2006b).

Since 1997, through various projects and programs, NASA has funded the collection of ocean *in situ* data for satellite data product validation, algorithm development, satellite data comparison and inter-calibration, and data merger studies and time series analyses. The SeaWiFS Bio-optical Archive and Storage System (SeaBASS) (Werdell et al., 2003; Werdell and Bailey, 2005) maintains a local repository of *in situ* ocean optical and bio-optical data to support and sustain regular scientific analyses. Specifically, the database includes *in situ* ocean optical (e.g., ocean water-leaving radiance spectra), biological (e.g., chlorophyll-a concentration), and other related oceanographic and atmospheric data (see details in http://seabass.gsfc.nasa.gov/). In fact, the SeaBASS data were contributed by a variety of researchers from international ocean community, using various instrumentation with all measurements closely follow rigorous, community-defined deployment and data processing protocols (Mueller and Fargion, 2002). The SeaBASS *in situ* data have been continuously used in support of SeaWiFS and MODIS ocean color product validation and algorithm evaluation, e.g., (Bailey and Werdell, 2006; Wang et al., 2005). Thus, the SeaBASS data are appropriate for the new algorithm evaluations.

In this paper, we evaluate the performance of three different MODIS ocean color data processing approaches, i.e., the NASA standard (NIR) algorithm, the SWIR algorithm, and the NIR–SWIR combined method, using the SeaBASS *in situ* data. Our purpose is to assess the algorithm performance for the SWIR and the NIR–SWIR combined methods in comparison to the standard (NIR) method. It is particularly useful to evaluate and understand the SWIR algorithm performance for producing the MODIS ocean color products (including particularly the SWIR algorithm performance in open oceans). The specific ocean color products utilized for this evaluation include MODIS-derived normalized water-leaving radiance (Gordon, 1997, 2005; Gordon and Wang, 1994; Morel and Gentili, 1991; Wang, 2006a), $nLw(\lambda)$, at wavelengths 412, 443, 488, 531, 551, and 667 nm, chlorophyll-a concentration (O'Reilly et al., 1998), Chl-a, and the diffuse attenuation coefficient (Mueller, 2000) at the wavelength 490 nm, *K490*. It is noted that the normalized water-leaving radiance data are essential for all satellite ocean biological and ocean optical products, e.g., chlorophyll-a concentration, the diffuse attenuation coefficient, and ocean inherent optical property data (Lee et al., 2002; Maritorena et al., 2002; Mueller, 2000; O'Reilly et al., 1998). We provide here the match-up method and detailed data analyses and discussions for the algorithm evaluation and validation. In addition, we show comparison results for some MODIS global monthly composite images of ocean color product derived using the standard (NIR), SWIR, and NIR–SWIR combined methods.

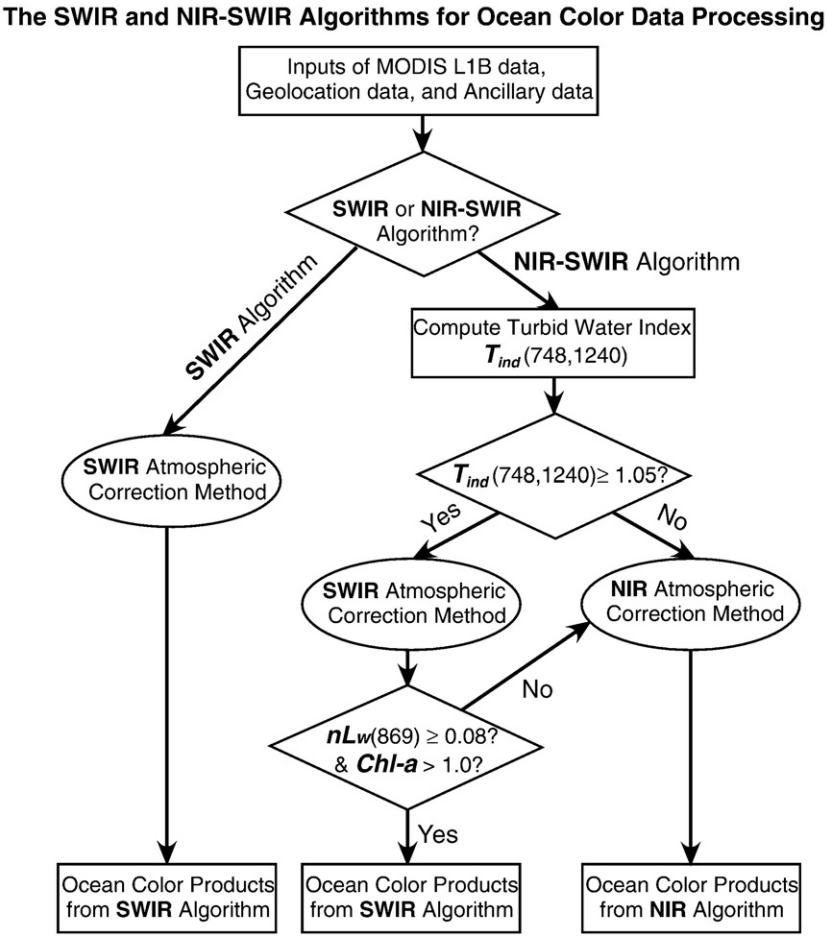

Fig. 1. The flow chart of the SWIR and NIR–SWIR atmospheric correction algorithms for MODIS ocean color data processing. Note that *nLw*(869) and Chl-a in the flow chart are in mW cm^{-2} μm^{-1} sr^{-1} and mg m^{-3}, respectively.

2. MODIS products compared with the *in situ* measurements

2.1. Data and method

The NIR, SWIR, and NIR–SWIR combined atmospheric correction algorithms have been described in detail in various references (Gordon and Wang, 1994; Gordon, 1997; Wang and Shi, 2005; Wang, 2007; Wang et al., 2007). For the NIR–SWIR combined method, however, there are some algorithm refinements for detection and identification of the turbid waters as compared with the original Wang and Shi (2007) method. Specifically, MODIS-measured pixels are identified as the turbid waters for cases with turbid water index (Shi and Wang, 2007) $T_{ind}(748,1240) > 1.05$ and normalized water-leaving radiance at the MODIS 869 nm ($nLw(869)$) ≥0.08 mW cm^{-2} μm^{-1} sr^{-1}, as well as

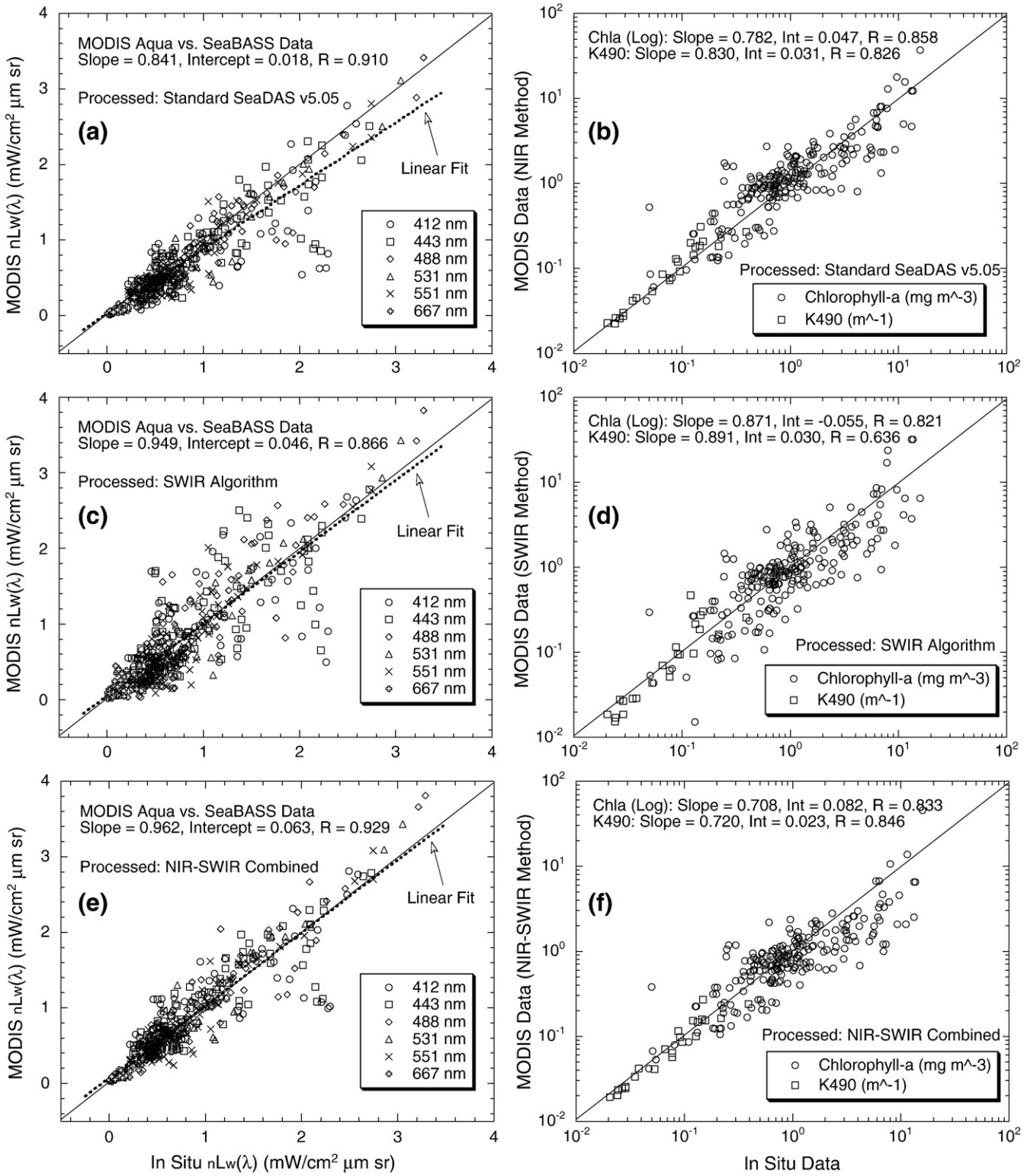

Fig. 2. MODIS-derived $nLw(\lambda)$, Chl-a and *K490* compared with *in situ* measurements using (a) and (b) the standard algorithm, (c) and (d) the SWIR algorithm, and (e) and (f) the NIR–SWIR combined method.

Chl-a value >1.0 mg/m^3. Thus, in the MODIS ocean color data processing, for pixels with turbid water index T_{ind}(748,1240) >1.05, one iteration of the SWIR atmospheric correction procedure is required for deriving the *nLw*(869) and Chl-a values. We found that this refinement improved the results in detecting the turbid water pixels, as well as MODIS-derived ocean color products. In the NIR–SWIR combined method, for pixels identified as turbid waters the SWIR algorithm is operated, while for all other pixels the NIR algorithm is executed (Wang and Shi, 2007). The NIR algorithm has employed a NIR ocean contribution correction (Stumpf et al., 2003) for the productive ocean waters. Fig. 1 provides the flow chart for the SWIR and NIR–SWR atmospheric correction algorithm procedures for the MODIS ocean color data processing.

It is also noted that the cloud-masking scheme implemented in the SWIR and NIR–SWIR algorithms for the ocean color data processing is different from that in the standard (NIR) algorithm (Wang and Shi, 2006). Both the SWIR and NIR–SWIR algorithms use the TOA reflectance at the MODIS SWIR 1240 nm band for cloud masking, while the standard (NIR) method uses the TOA NIR 869 nm reflectance for identifying clear sky scenes. The SWIR cloud-masking algorithm generally has a better performance than the NIR algorithm in the coastal ocean regions (Wang and Shi, 2006). Detailed comparisons and discussions in the cloud-masking algorithm performance for the NIR and SWIR reflectance approaches can be found in Wang and Shi (2006). In addition, the improved aerosol lookup tables that include aerosol polarization effects have been implemented in the SWIR and NIR–SWIR algorithms (Wang, 2006b), and both algorithms have been vicariously calibrated based on a scheme outline in (Wang, 2006b).

MODIS-Aqua standard level-2 data have been compared with *in situ* measurements from the SeaBASS database for the period of 2002–2005, following Bailey and Werdell (2006). The match-up results between MODIS-Aqua and SeaBASS *in situ* data are available from the NASA ocean color website (http://oceancolor.gsfc.nasa.gov), and used here as a reference. The same SeaBASS data set is also used for the algorithm evaluation for the SWIR and NIR–SWIR combined methods. MODIS ocean color products that are processed using the SWIR and NIR–SWIR algorithms are generated from the MODIS-Aqua level-1B data. While the match-up results in the NASA ocean color website were produced using the SeaWiFS Data Analysis System (SeaDAS) version 4.8 for MODIS-Aqua data processing, the current MODIS ocean color products are processed using SeaDAS version 5.05. We have verified that results produced from these two SeaDAS versions are consistent (with small differences). Thus, in this study there are three MODIS-Aqua product data sets that are compared with the SeaBASS *in situ* data: the NASA standard products processed using the SeaDAS version 5.05 (data downloaded directly from NASA ocean color web site http://oceancolor.gsfc.nasa.gov), the products produced using the SWIR algorithm, and the data from the NIR–SWIR combined method (data processed from MODIS L1B for both the SWIR and NIR–SWIR methods).

The *in situ* data used in this study are from the SeaBASS data sets that were collected by various investigators during 2002–2005. Specifically, the *in situ* data discussed and used in the match-up analyses in here were primarily from ocean regions of the U.S. east coast (42°N–44°N, 70°W–76°W), the U.S. west coast (34°N–37°N, 117°W–124°W), the Adriatic Sea (12°N–16°N, 12°E–16°E), and the Brazilian east coast (27°S–50°S, 45°W–60°W). Some small portion of the *in situ* data was from the North Pacific (near Hawaii), south west coast of Africa, east coast of Africa, and the South China Sea. In the satellite and *in situ* data match-up analyses, ~10% of the *in situ* radiance data used in this study may be considered as from turbid ocean waters, i.e., at least one pixel from the satellite 5×5 match-up box (see below) is characterized as the turbid water and processed using the SWIR algorithm in the NIR–SWIR data processing (Fig. 1).

For the data match-up analyses, the procedure of Bailey and Werdell (2006) was used to produce the satellite data for comparison with the *in situ* measurements. Briefly, for a given MODIS-derived ocean color product, pixels with a 5×5 box centered at the location of the *in situ* measurement were extracted. A set of masks was used to produce the valid ocean color products in MODIS data processing. These exclusion masks are: land, cloud/ice, stray light, and sun glint. In addition, two flags were also used to exclude pixels with high solar-zenith angle (>75°) and/or sensor-zenith angle (>60°). A valid satellite match-up requires a minimum of 50% valid pixels in the defined 5×5 box (i.e., ≥13 valid pixels). Furthermore, a uniformity screen for the defined match-up box is applied for producing the mean value (Bailey and Werdell, 2006). Specifically, the mean value ($\overline{Y}$) and standard deviation (STD) from the defined match-up box are first computed. A filter of ($\overline{Y}\pm1.5\times$STD) is then defined to further select the required pixels from the 5×5 box for a revised mean value and STD computations, i.e., pixels with their values between ($\overline{Y}-1.5\times$STD) and ($\overline{Y}+1.5\times$STD) are used for deriving the final mean value and other statistics parameters (e.g., STD). In addition, the data match-ups are only considered for cases where the time difference between the satellite and *in situ* measurements is within three (±3) hours.

2.2. Overall comparison results

Fig. 2 provides an overall comparison between the MODIS-derived and *in situ* measured ocean color products for various cases. The ocean color products included in these results are the normalized water-leaving radiance *nLw*(λ) at wavelengths 412, 443, 488, 531, 551, and 667 nm, chlorophyll-a concentration (Chl-a), and the diffuse attenuation coefficient at the wavelength 490 nm (*K490*). Fig. 2(a), (c), and (e) show *nLw*(λ) comparisons, while Fig. 2(b), (d), and (f) are evaluations

Table 1
The match-up comparisons for the various ocean color products as in the slope, intercept (Int), and correlation coefficient (*R*)

Product	Data #	Standard method			SWIR method			NIR-SWIR method		
		Slope	Int[a]	*R*[b]	Slope	Int[a]	*R*[b]	Slope	Int[a]	*R*[b]
nLw(412)	86	0.700	0.064	0.793	0.727	0.216	0.727	0.758	0.253	0.839
nLw(443)	98	0.770	0.092	0.859	0.851	0.155	0.772	0.864	0.172	0.885
nLw(488)	93	0.916	−0.008	0.936	1.104	−0.059	0.892	1.038	0.039	0.940
nLw(531)	27	0.932	−0.032	0.952	1.084	−0.110	0.950	1.060	0.017	0.957
nLw(551)	94	0.915	0.000	0.952	1.085	−0.076	0.914	1.047	0.025	0.959
nLw(667)	66	0.632	0.007	0.771	0.757	0.065	0.435	0.771	0.019	0.803
Overall *nLw*(λ)	464	0.841	0.018	0.910	0.949	0.046	0.866	0.962	0.063	0.929
K490	23	0.830	0.031	0.826	0.891	0.030	0.636	0.720	0.023	0.846
Chl-a[c]	224	0.782	0.047	0.858	0.871	−0.055	0.821	0.708	0.082	0.833

[a] Intercept for line fit.
[b] Correlation coefficient.
[c] Data fitted in log scale.

for products Chl-a and *K490*. Fig. 2(a), (c), and (e) are MODIS-derived *nLw*(λ) results compared with the *in situ* measurements, corresponding to cases for which MODIS-Aqua data are processed using the standard (NIR), SWIR, and NIR–SWIR combined method, respectively. Fig. 2(b), (d), and (f) are results of the Chl-a and *K490* match-ups corresponding to MODIS data processed with the three different algorithms.

For the *nLw*(λ) results, the slopes of the overall match-ups using the SWIR and NIR–SWIR methods (Fig. 2(c) and (e)) have been improved compared with those using the standard (NIR) method

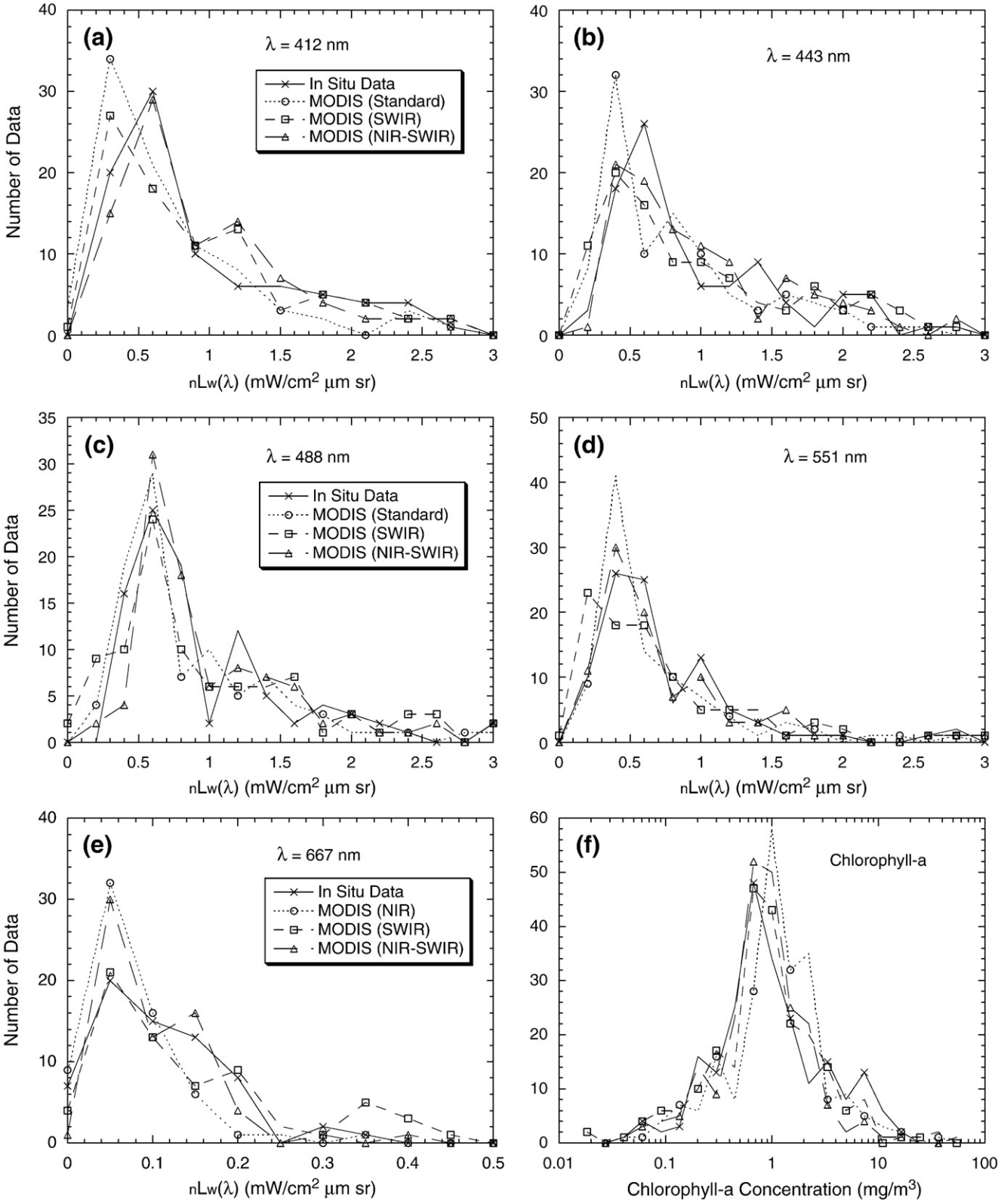

Fig. 3. Comparisons of the histogram results in the ocean color products from the *in situ* data and from the MODIS measurements with three different methods for (a)–(e) *nLw*(λ) at the wavelength 412, 443, 488, 551, and 667 nm, respectively, and (f) chlorophyll-a concentration.

(Fig. 2(a)). However, the SWIR method produced increased product noise, which can be seen in Fig. 2 and is also indicated from the reduced correlation coefficient for the match-ups. The slopes in the overall *nLw*(λ) match-ups for the standard, SWIR, and NIR–SWIR methods are 0.841, 0.949, and 0.962 with their corresponding correlation coefficients of 0.910, 0.866, and 0.929, respectively. The data noise produced by the SWIR method is due mainly to the substantially lower sensor SNR values for the MODIS SWIR bands and also because of SWIR algorithm performance errors (Wang, 2007). Similar results are also shown for the Chl-a and *K490* match-up comparisons (Fig. 2(b), (d), and (f)); in particular, results from the SWIR method show lower correlation coefficient values.

Table 1 summarizes match-up values of the slope, intercept (Int), and correlation coefficient (R) for the *nLw*(λ) at various wavelengths, as well as results for the *nLw*(λ) overall comparison. The match-up comparisons (slope, intercept, and correlation coefficient) for products Chl-a and *K490* are also provided in Table 1. The number of data (same for all three methods) that are used for the match-up analyses are provided in Table 1. For the slope comparison, the results in Table 1 show that overall the SWIR and NIR–SWIR methods performed slightly better than the standard method. However, the SWIR method produced a little more data noise as indicated by the lower values in correlation coefficients. The match-up results from the NIR–SWIR method have correlation coefficient values that are comparable to those from the standard method.

Fig. 3 compares histograms of the ocean color data products from the SeaBASS database (*in situ* measurements) to the MODIS data derived from three different approaches. Fig. 3(a)–(e) are histogram results for the normalized water-leaving radiance *nLw*(λ) at wavelengths 412, 443, 488, 551, and 667 nm, respectively, while Fig. 3(f) is results for the chlorophyll-a comparisons. The histogram results in the *nLw*(λ) comparison show that, compared with the *in situ* data, the standard (NIR) method produces biased low *nLw*(λ) at the blue bands, while the SWIR method generally has a slightly larger data range in the MODIS derived products. On the other hand, the chlorophyll-a results derived from the standard (NIR) method (Fig. 3(f)) show an overall slightly biased high value (data peak at ~1 mg/m^3) compared with the *in situ* data, while results from both SWIR and NIR–SWIR combined methods appear match well with the *in situ* chlorophyll-a data.

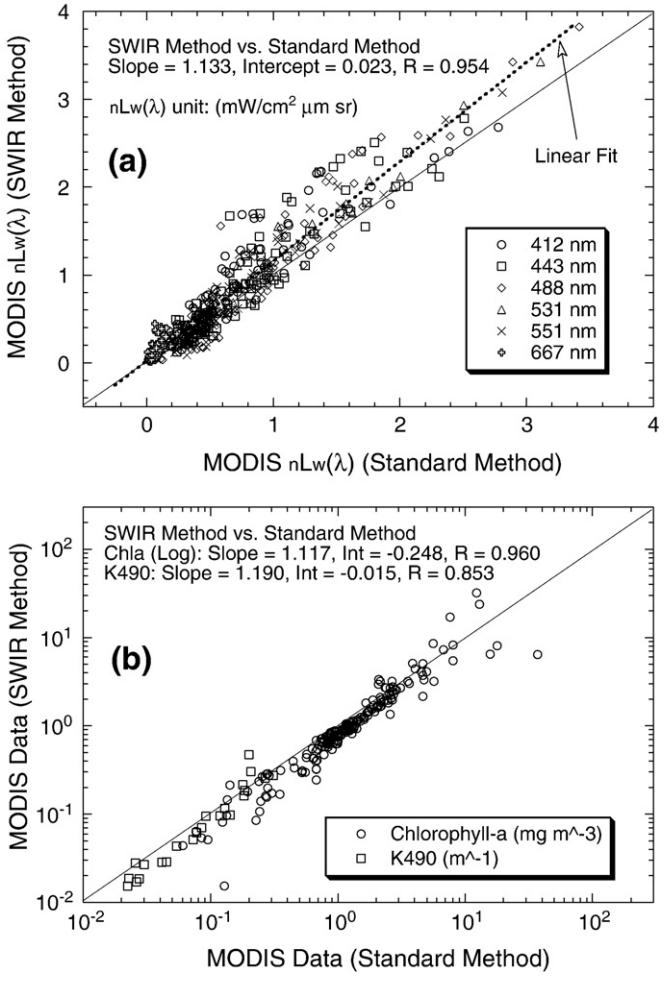

Fig. 4. Comparisons of the MOIDS ocean color products derived using the SWIR and standard (NIR) algorithms for (a) *nLw*(λ) data and (b) Chl-a and *K490* products.

Table 2
Results of the mean ratio value (MODIS vs. *in situ*) and standard deviation (STD) for various MODIS ocean color products derived using three different algorithms

Product	Data #	Mean ratio[a]±STD[b]		
		Standard method	SWIR method	NIR–SWIR method
nLw(412)	86	0.804±0.351	1.058±0.585	1.163±0.418
nLw(443)	98	0.898±0.294	1.062±0.548	1.114±0.335
nLw(488)	93	0.907±0.233	1.026±0.442	1.103±0.260
nLw(531)	27	0.929±0.252	0.974±0.307	1.073±0.279
nLw(551)	94	0.939±0.236	0.957±0.384	1.019±0.243
nLw(667)	66	0.762±0.389	1.542±1.213	1.056±0.479
K490	23	1.163±0.293	1.124±0.713	0.976±0.248
Chl-a	224	1.359±1.081	1.135±0.904	1.037±0.828

[a]Mean ratio between MODIS vs. *in situ* data.
[b]Standard deviation.

Providing an overall SWIR algorithm performance evaluation in a reference to the standard method, Fig. 4 shows comparisons of the MODIS-derived products using the SWIR (*y*-axis) and standard (NIR) (*x*-axis) algorithm. Fig. 4(a) provides comparisons of the derived *nLw*(λ) values, while Fig. 4(b) compares results of Chl-a and *K490* products. The overall *nLw*(λ) comparisons (Fig. 4(a)) show a linear fit with a slope of 1.133, an intercept of 0.023, and the correlation coefficient of 0.954. Therefore, overall the MODIS *nLw*(λ) values derived using the SWIR method are generally slightly larger than those using the standard (NIR) method. Some data dispersion in Fig. 4(a) is also apparent, due to data noise from the SWIR method. Both Chl-a and *K490* results in Fig. 4(b) indicate slightly lower values derived from the SWIR method when compared with those from the standard (NIR) algorithm (data are mostly under 1:1 line). The fit for Chl-a (in logarithmic scale) has a slope of 1.117 (>1), but with an intercept of −0.248 (<0). On the other hand, a linear fit for the *K490* comparison has a slope, intercept, and correlation coefficient of 1.190 (>1), −0.015 (<0), and 0.853, respectively. It is noted that the Chl-a comparison shows a high correlation coefficient (0.960), indicating the reduced noise error in the Chl-a data (proportional to the ratio of *nLw*(λ) values at two bands) from the SWIR method.

2.3. Some quantitative comparisons and evaluations

2.3.1. Mean ratio results between satellite and in situ data

For a more quantitative evaluation, the mean ratio value between the MODIS-derived products (from the three different approaches) and the *in situ* measured data are computed, as well as the corresponding STD values. Table 2 shows results of the mean ratio values and STDs for the MODIS-Aqua products processed using the standard (NIR), SWIR, and NIR–SWIR methods compared with the SeaBASS *in situ* data. In Table 2, the mean ratio value between the MODIS-derived vs. *in situ* data, as well as the corresponding STD from the standard, SWIR, and NIR–SWIR methods are provided for *nLw*(λ) at wavelengths 412, 443, 488, 531, 551, 667 nm, the diffuse attenuation coefficient *K490*, and chlorophyll-a concentration Chl-a. Table 2 also provides the number of data (same for all three

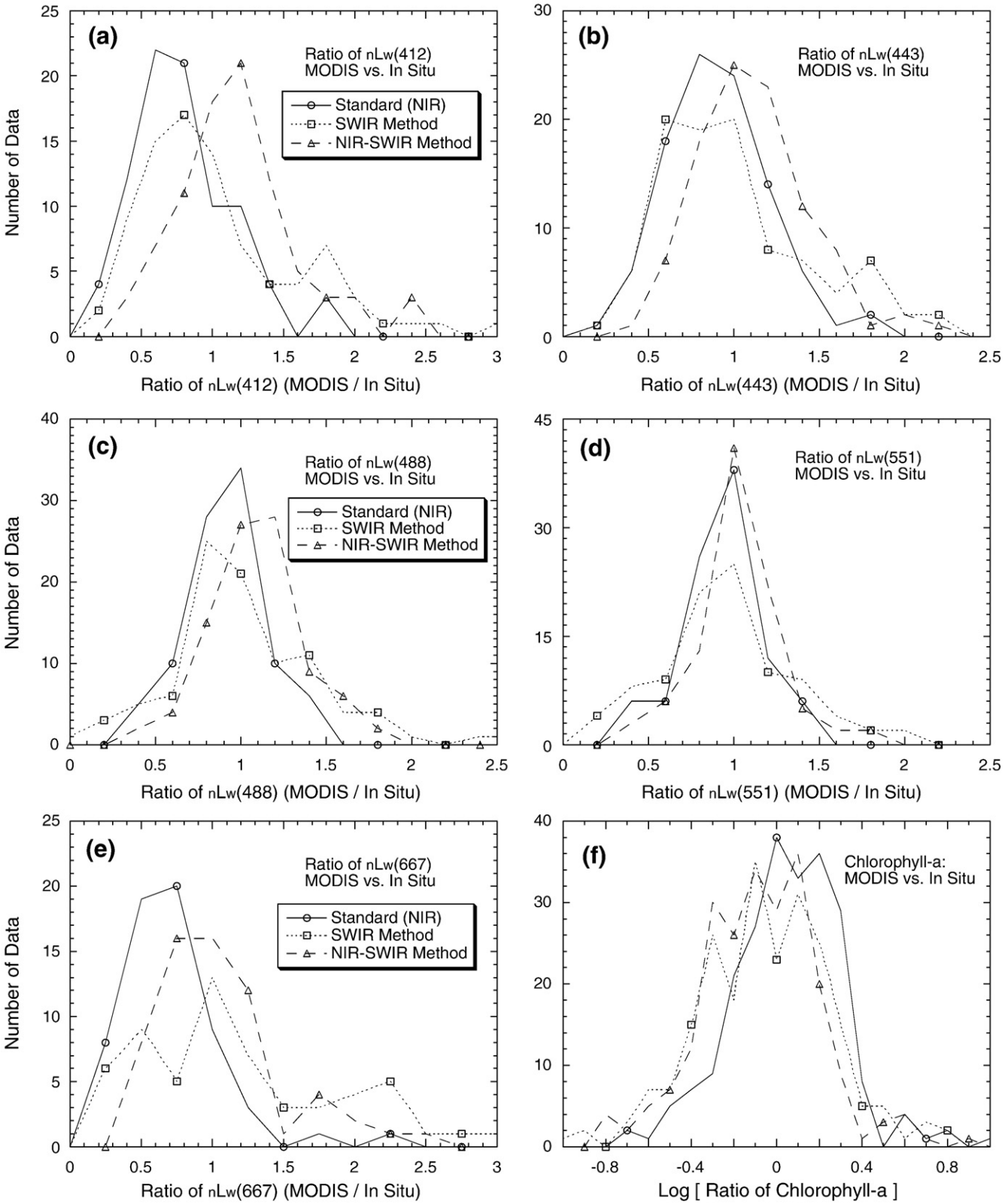

Fig. 5. Comparisons of histogram results in the ratio value (MODIS vs. *in situ*) with the MODIS data processed using the standard (NIR), SWIR, and NIR–SWIR methods for (a)–(e) ratio of $nLw(\lambda)$ at the wavelength 412, 443, 488, 551, and 667 nm, respectively, and (f) ratio of chlorophyll-a (in logarithmic scale).

methods) that are used for the mean ratio and STD computations for each parameter.

Results in Table 2 show that overall the SWIR method produced radiance data with the lowest bias errors, but with the highest noise. Compared with products derived from the standard method, products from the SWIR method generally have higher noise, in particular, for the $nLw(\lambda)$ data at the blue bands. For the $nLw(412)$ comparison, even though the SWIR method produced improved data quality with regard to the bias error, the data noise from the SWIR method is significantly increased compared with results from

the standard method. Conversely, results from the standard method show a generally biased low error in $nLw(\lambda)$ product and biased high error in *K490* and Chl-a data. The $nLw(\lambda)$ product from the NIR–SWIR method has a slightly biased high error with the STD values comparable with those from the standard method. For this exercise, however, the NIR–SWIR method produced the best *K490* and Chl-a products with the mean ratio and STD of 0.976±0.248 and 1.037±0.828, respectively.

2.3.2. Histogram results

Fig. 5 shows histogram results in the ratio value between MODIS-derived and *in situ* measured data, demonstrating error distribution for the three algorithms for various ocean color products. Fig. 5(a)–(e) are histogram results in $nLw(\lambda)$ at wavelengths of 412, 443, 488, 551, and 667 nm, respectively, while Fig. 5(f) shows results for the chlorophyll-a ratio (in logarithmic scale). For the $nLw(\lambda)$ comparisons, Fig. 5(a) and (b) show the peak values for $nLw(\lambda)$ ratio at wavelengths 412 and 443 nm are biased low (<1) for the data from the standard (NIR) algorithm, while the data processed using the SWIR algorithm show a large variation (histogram data spread more widely). On the other hand, the chlorophyll-a results (Fig. 5(f)) show comparable data variations in the ratio values from all three methods, but with slightly higher ratio derived from the standard (NIR) method. These results are consistent with results discussed in the previous sections.

3. Discussions

The match-up analysis demonstrates that using the MODIS SWIR bands for ocean color data processing has reduced the bias errors in $nLw(\lambda)$. However, the noise errors are increased, possibly leading to some negative $nLw(\lambda)$ cases for which true $nLw(\lambda)$ values are very low. Comparing to the results from the standard (NIR) method, however, the SWIR method improves the MODIS-derived $nLw(\lambda)$ products in the coastal regions, where true $nLw(\lambda)$ values at the blue

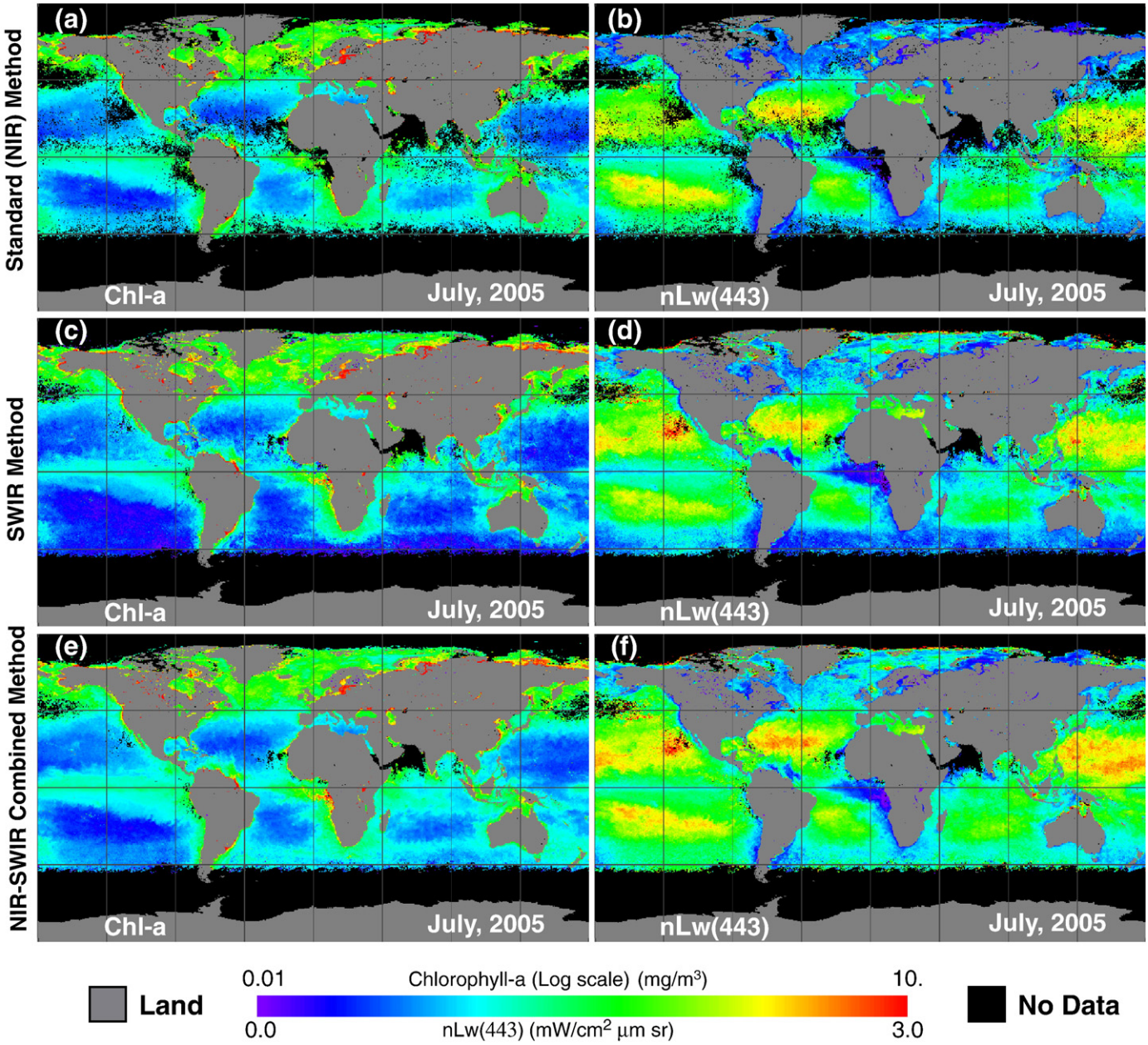

Fig. 6. Color images for the global composite distribution of the MODIS-Aqua derived Chl-a and $nLw(443)$ for the month of July 2005, which were retrieved using (a) and (b) the standard (NIR) algorithm, (c) and (d) the SWIR method, and (e) and (f) the NIR–SWIR combined method.

(412 and 443 nm) are often quite low. In these cases, we found that using the SWIR method the MODIS $nLw(\lambda)$ values at the blue are elevated (Wang and Shi, 2007; Wang et al., 2007) and cases with the negative $nLw(\lambda)$ are in fact reduced significantly. Therefore, in the coastal ocean regions, the SWIR method is usually superior to the NIR method, particularly over the turbid waters. It is important to note that, for both the SWIR and NIR–SWIR algorithms, bias errors in $nLw(\lambda)$ from the match-up analysis are reduced, indicating improved algorithm performance also related to the improved aerosol lookup tables with the vicarious calibration.

The data product noise errors from the SWIR method are mainly from two sources: (1) considerably lower SNR values for the MODIS SWIR bands that are used for the data processing (atmospheric correction) and (2) a little more uncertainty introduced by using the SWIR bands (1240 and 2130 nm) for atmospheric correction. A recent study (Wang, 2007) shows that atmospheric correction using the SWIR bands (1240 and 2130 nm) for deriving $nLw(\lambda)$ often produces a little larger uncertainty than results from the NIR bands (748 and 869 nm). This is particularly true for cases of the maritime aerosols, which are often dominated in the open oceans. In addition, with the current MODIS SNR characteristics for the SWIR bands, there is significant noise in the derived $nLw(\lambda)$ using the SWIR algorithm (Wang, 2007). Therefore, it is proposed that MODIS-Aqua ocean color products be processed using the NIR–SWIR combined method for which the non-turbid and turbid ocean waters are processed using the standard (NIR) and SWIR method, respectively.

For the turbid coastal waters, the use of the MODIS SWIR algorithm versus the standard (NIR) algorithm with the NIR ocean contribution correction is somewhat a tradeoff between using a noised measurement with little or no bias versus a high quality radiance measurement with a correction algorithm that is in error. However, it is generally desired to use the satellite-measured data instead of modeling for the NIR ocean contribution correction because of model limitations, particularly over very turbid waters. A recent study (paper in preparation) shows that, for extremely turbid waters, it is difficult to model the NIR ocean contributions. Thus, the SWIR algorithm is still required for the coastal and inland turbid waters.

4. Comparisons from MODIS-Aqua global data processing

The standard (NIR), SWIR, and NIR–SWIR algorithm performances are further evaluated with the MODIS-Aqua global ocean color product data. Fig. 6 provides color images for global composite distributions of MODIS-Aqua Chl-a and $nLw(443)$ for the month of July 2005, which were derived using the standard (NIR), SWIR, and NIR–SWIR combined methods from MODIS-Aqua global measurements. Fig. 6(a), (c), and (d) are color images of Chl-a for MODIS-Aqua data that were processed using the standard (NIR), SWIR, and NIR–SWIR method, respectively, while Fig. 6(b), (d), and (f) are the corresponding $nLw(443)$ images from the three different data processing methods. The product images for the standard (NIR) method (Fig. 6(a) and (b)) were downloaded directly from the NASA ocean color website, while results of the SWIR and NIR–SWIR combined methods (Fig. 6(c)–(f)) were generated from the MODIS-Aqua L1B data (July of 2005) using the SWIR and NIR–SWIR method, respectively. These images compare the global spatial variations of the ocean color products (Chl-a and $nLw(443)$) that were derived from three different methods. It is noted that there is a solar-zenith angle cut off at 70° for all three data processing methods. Results in Fig. 6 show that, for the most of ocean regions, all three methods produced similar monthly Chl-a and $nLw(443)$ data distributions. However, Fig. 6 shows some obvious differences in MODIS-derived Chl-a and $nLw(443)$ from three methods. Both SWIR and NIR–SWIR methods show some improved data coverage, e.g., along the China east coastal region, while the SWIR method produced some obvious different results in some open ocean regions, e.g., in the southern ocean. Judging data quality by their coverage, spatial continuity, and image smoothness, it appears that the NIR–SWIR method produced the best Chl-a and $nLw(443)$ results.

5. Conclusions

Using the *in situ* measurements from the SeaBASS database, we have evaluated MODIS-Aqua ocean color products derived from the atmospheric correction algorithm using the standard (NIR), SWIR, and NIR–SWIR combined methods. Results show that, although the bias errors in the derived $nLw(\lambda)$ are reduced using the SWIR method, there is increased noise in the derived $nLw(\lambda)$ product due primarily to considerably lower sensor SNR values for the MODIS SWIR bands and also because of errors from the SWIR algorithm. Therefore, for accurate ocean color products, future ocean color satellite sensors will require much better sensor SNR performance for the SWIR bands. Conversely, results from the NIR–SWIR algorithm evaluation demonstrate improved ocean color products, particularly, for the chlorophyll-a product. Therefore, it is suggested that for the non-turbid ocean the MODIS ocean color products be processed using the NIR algorithm, while for the coastal turbid waters the data be processed using the SWIR and/or other methods to account for significant NIR ocean contributions.

Acknowledgments

This research was supported by the NASA and NOAA funding and grants. The authors are grateful to the all scientists who have contributed valuable data to SeaBASS database; for this study, the *in situ* data were contributed by Annick Bricaud, William Balch, Ken Carder, Francisco Chavez, Carlos Garcia, Greg Mitchell, Norman Nelson, David Siegel, and Rick Stumpf. We also thank the NASA Ocean Biology Processing Group for maintaining and distributing the SeaBASS database. We thank two anonymous reviewers for their useful comments. The MODIS L1B data and Level-2 ocean color products were obtained from NASA/GSFC MODAPS Services website and Ocean Color website, respectively. The views, opinions, and findings contained in this paper are those of the authors and should not be construed as an official NOAA or U.S. Government position, policy, or decision.

References

Bailey, S. W., & Werdell, P. J. (2006). A multi-sensor approach for the on-orbit validation of ocean color satellite data products. *Remote Sensing Environment*, *102*, 12–23.
Franz, B.A., Werdell, P.J., Meister, G., Kwiatkowska, E.J., Bailey, S.W., Ahmad, Z., & McClain, C.R., (2006), MODIS land bands for ocean remote sensing applications, paper presented at Ocean Optics XVIII, Montreal, Canada, Oct. 9-13.
Gordon, H. R. (1997). Atmospheric correction of ocean color imagery in the Earth Observing System era. *Journal Geophysical Research*, *102*, 17,081–017,106.
Gordon, H. R. (2005). Normalized water-leaving radiance: revisiting the influence of surface roughness. *Applied Optics*, *44*, 241–248.
Gordon, H. R., & Wang, M. (1994). Retrieval of water-leaving radiance and aerosol optical thickness over the oceans with SeaWiFS: a preliminary algorithm. *Applied Optics*, *33*, 443–452.
Lavender, S. J., Pinkerton, M. H., Moore, G. F., Aiken, J., & Blondeau-Patissier, D. (2005). Modification to the atmospheric correction of SeaWiFS ocean color images over turbid waters. *Continental Shelf Research*, *25*, 539–555.
Lee, Z. P., Carder, K. L., & Arnone, R. A. (2002). Deriving inherent optical properties from water color: a multiple quasi-analytical algorithm for optically deep waters. *Applied Optics*, *41*, 5755–5772.
Maritorena, S., Siegel, D. A., & Peterson, A. (2002). Optimization of a semi-analytical ocean color model for global scale applications. *Applied Optics*, *41*, 2705–2714.
McClain, C. R., Feldman, G. C., & Hooker, S. B. (2004). An overview of the SeaWiFS project and strategies for producing a climate research quality global ocean bio-optical time series. *Deep-Sea Research Part 2. Topical Studies in Oceanography*, *51*, 5–42.
Morel, A., & Gentili, G. (1991). Diffuse reflectance of oceanic waters: its dependence on Sun angle as influenced by the molecular scattering contribution. *Applied Optics*, *30*, 4427–4438.
Mueller, J. L. (2000). SeaWiFS algorithm for the diffuse attenuation coefficient, K(490), using water-leaving radiances at 490 and 555 nm. In S. B. Hooker & E. R. Firestone (Eds.), *NASA Tech. Memo. 2000-206892SeaWiFS Postlaunch Technical Report Series*, *Vol. 11.* (pp. 24–27) Greenbelt, Maryland: NASA Goddard Space Flight Center.
Mueller, J. M., & Fargion, G. S. (2002). Ocean optics protocols for satellite ocean color sensor validation. *Revision 3, Part I & II,NASA Tech. Memo. 2002–210004, p1-308* Greenbelt, Maryland: NASA Goddard Space Flight Center.

O'Reilly, J. E., Maritorena, S., Mitchell, B. G., Siegel, D. A., Carder, K. L., Garver, S. A., Kahru, M., & McClain, C. R. (1998). Ocean color chlorophyll algorithms for SeaWiFS. *Journal of Geophysical Research*, *103*, 24,937–924,953.

Ruddick, K. G., Ovidio, F., & Rijkeboer, M. (2000). Atmospheric correction of SeaWiFS imagery for turbid coastal and inland waters. *Applied Optics*, *39*, 897–912.

Shi, W., & Wang, M. (2007). Detection of turbid waters and absorbing aerosols for the MODIS ocean color data processing. *Remote Sensing Environment*, *110*, 149–161.

Siegel, D. A., Wang, M., Maritorena, S., & Robinson, W. (2000). Atmospheric correction of satellite ocean color imagery: the black pixel assumption. *Applied Optics*, *39*, 3582–3591.

Stumpf, R. P., Arnone, R. A., Gould, R. W., Martinolich, P. M., & Ransibrahmanakul, V. (2003). A partially coupled ocean-atmosphere model for retrieval of water-leaving radiance from SeaWiFS in coastal waters. In S. B. Hooker & E. R. Firestone (Eds.), *NASA Tech. Memo. 2003-206892SeaWiFS Postlaunch Technical Report Series*, *Vol. 22*. (pp. 51–59) Greenbelt, Maryland: NASA Goddard Space Flight Center.

Wang, M. (2006). Effects of ocean surface reflectance variation with solar elevation on normalized water-leaving radiance. *Applied Optics*, *45*, 4122–4128.

Wang, M. (2006). Aerosol polarization effects on atmospheric correction and aerosol retrievals in ocean color remote sensing. *Applied Optics*, *45*, 8951–8963.

Wang, M. (2007). Remote sensing of the ocean contributions from ultraviolet to near-infrared using the shortwave infrared bands: simulations. *Applied Optics*, *46*, 1535–1547.

Wang, M., Knobelspiesse, K. D., & McClain, C. R. (2005). Study of the Sea-Viewing Wide Field-of-View Sensor (SeaWiFS) aerosol optical property data over ocean in combination with the ocean color products. *Journal of Geophysical Research*, *110*, D10S06. doi:10.1029/2004JD004950

Wang, M., & Shi, W. (2005). Estimation of ocean contribution at the MODIS near-infrared wavelengths along the east coast of the U.S.: two case studies. *Geophysical Research Letters*, *32*, L13606. doi:10.1029/2005GL022917

Wang, M., & Shi, W. (2006). Cloud masking for ocean color data processing in the coastal regions. *IEEE Transaction on Geoscience and Remote Sensing*, *44*, 3196–3205.

Wang, M., & Shi, W. (2007). The NIR–SWIR combined atmospheric correction approach for MODIS ocean color data processing. *Optics Express*, *15*, 15722–15733.

Wang, M., Tang, J., & Shi, W. (2007). MODIS-derived ocean color products along the China east coastal region. *Geophysical Research Letters*, *34*, L06611. doi:10.1029/2006GL028599

Werdell, P. J., & Bailey, S. W. (2005). An improved in-situ bio-optical data set for ocean color algorithm development and satellite data product validation. *Remote Sensing of Environment*, *98*, 122–140.

Werdell, P. J., Bailey, S., Fargion, G., Pietras, C., Knobelspiesse, K., Feldman, G., & McClain, C. R. (2003). Unique data repository facilitates ocean color satellite validation. *Eos, Transactions, American Geophysical Union* (pp. 377).